Journal of Power Sources 185 (2008) 1340–1347

Contents lists available at ScienceDirect

Journal of Power Sources

journal homepage: www.elsevier.com/locate/jpowsour

A self-catalytic mixed-conducting membrane reactor for effective production of hydrogen from methane

Xueliang Dong, Zhengkun Liu, Wanqin Jin*, Nanping Xu

State Key Laboratory of Materials-Oriented Chemical Engineering, College of Chemistry and Chemical Engineering, Nanjing University of Technology, 5 Xinmofan Road, Nanjing 210009, PR China

ARTICLE INFO

Article history:
Received 27 June 2008
Received in revised form 7 August 2008
Accepted 20 August 2008
Available online 30 August 2008

Keywords:
Supported membrane
Co-sintering
Self-catalytic membrane reactor
Oxygen permeation
Hydrogen production
Fuel cell

ABSTRACT

A supported mixed-conducting LNCO membrane with a pore-gradient structure LNO support was successfully prepared via a dry pressing and co-sintering route. The match of sintering behaviors between membrane and support was realized by the preparation of an ABB′B″B′BA-type membrane. A scanning electron microscopy (SEM) test demonstrated that the surface of the supported membrane was dense and crack-free and the pore-gradient structure of the support can be observed clearly. The oxygen flux of the supported membrane was about 5.6 times that of the symmetric LNCO membrane. A self-catalytic mixed-conducting membrane reactor was constructed using the prepared membrane for hydrogen production from methane. It was found that this membrane reactor exhibited high performance and good stability for hydrogen production. At 1123 K, the CH_4 conversion, hydrogen selectivity and hydrogen production remained at about 60%, 89% and 8.0 ml(STP) cm^{-2} min^{-1}, respectively, for more than 120 h.

1. Introduction

Because of its high-energy conversion efficiency and low emission of air pollutants, the fuel cell holds promise for application as an energy source. Up to now, various types of fuel cell have been operated with hydrogen [1–3]. For successful commercialization, a stable supply of hydrogen is required at low cost and high efficiency [4]. During the past two decades, studies on hydrogen generation from various sources, such as fossil fuels, water and biomass, etc. have been extensively reported. However, it is generally accepted that hydrogen production will mainly rely on fossil fuels, primarily natural gas, for at least another half-century or so [5]. There are many techniques for converting natural gas to hydrogen [6–8]. Among these technologies, steam reforming is most commonly utilized [7], and can be represented by the reactions (1) and (2):

$$CH_4 + H_2O = CO + 3H_2 \quad \Delta H^0_{298} = 206\,kJ\,mol^{-1} \tag{1}$$

$$CO + H_2O = CO_2 + H_2 \quad \Delta H^0_{298} = -41.2\,kJ\,mol^{-1} \tag{2}$$

However, a high consumption of energy is inevitable due to the high endothermic nature of the reaction and the need to use excess steam to reduce carbon formation. An alternative process to produce hydrogen is the partial oxidation of methane (POM) using pure oxygen in the presence of a catalyst. This has greater selectivity and exothermicity [9], as represented by the reactions (3):

$$CH_4 + \frac{1}{2}O_2 = CO + 2H_2 \quad \Delta H^0_{298} = -36\,kJ\,mol^{-1} \tag{3}$$

The main difficulty with the POM process lies in the consumption of large quantities of expensive pure oxygen, which is produced by the cryogenic separation of air. Recently, an important advance in using air directly as a feedstock for the POM process has resulted from the application of a mixed-conducting oxide membrane reactor (with high oxygen ionic and electronic conductivities), which integrated the oxygen separation and POM processes in a single unit [10,11]. However, for this process, the performance of the membrane reactor is always restricted by the membrane permeability and catalytic activity.

In this work we propose a novel self-catalytic membrane reactor (SCMR) based on a supported mixed-conducting membrane to improve the performance of the membrane reactor. As depicted in Fig. 1, porous $La_2NiO_{4+\delta}$ (LNO), a mixed ionic–electronic conductor with catalytic activity for methane reforming [12], was used not only for the membrane support but also for the catalyst precursor. Considering the match of thermal performances between the membrane and the support, $La_2Ni_{0.9}Co_{0.1}O_{4+\delta}$ (LNCO) mixed-conducting oxide was selected as the membrane. The reduction of oxygen to oxygen ion occurs on the membrane side and the POM takes place simultaneously on the support side. At the start of the

* Corresponding author. Fax: +86 25 8358 7211.
E-mail address: wqjin@njut.edu.cn (W. Jin).

0378-7753/$ – see front matter © 2008 Elsevier B.V. All rights reserved.
doi:10.1016/j.jpowsour.2008.08.066

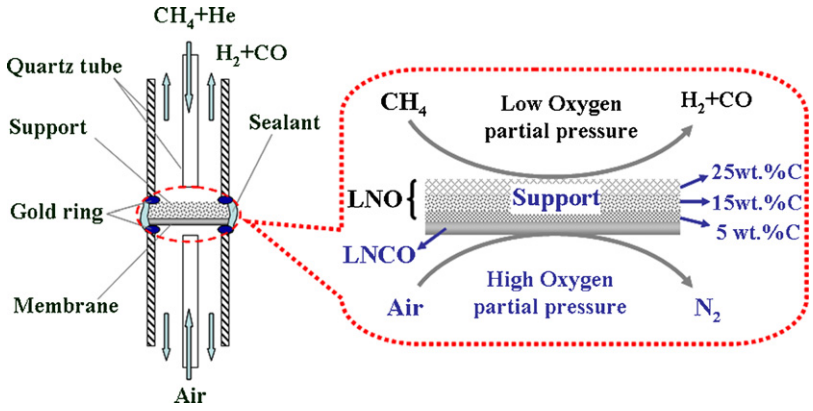

Fig. 1. Schematic diagram of the self-catalytic membrane reactor for hydrogen production.

POM reaction, CH_4 is partial oxidized by the porous support (LNO) to CO and H_2, and simultaneously parts of the LNO on the surface of the support were reduced to zero valent nickel (Ni^0) and La_2O_3 [13]. This process can be considered as a self-catalytic process because Ni^0 as the catalyst for the POM reaction can be produced during the reaction.

2. Experimental

2.1. Powder synthesis

The LNO and LNCO oxides were prepared via a gel-combustion method [14]. Analytical-grade La_2O_3, $Ni(NO_3)_2{\cdot}6H_2O$ and $Co(NO_3)_2{\cdot}6H_2O$ were used as the starting materials. For the synthesis of LNO oxide, La_2O_3 was dissolved in dilute nitric acid. An aqueous solution containing La and Ni ions then prepared by dissolving stoichiometric amounts of $La(NO_3)_3$ and $Ni(NO_3)_2{\cdot}6H_2O$ into a measured volume of deionized water under continuous agitation. The required amount of EDTA, dissolved in $NH_3{\cdot}H_2O$, was then dropped into the mixed metal nitrate solution, followed by the addition of solid citric acid whilst stirring; the mole ratio of total metal ions to EDTA and to citrate was 1:1:2. $NH_3{\cdot}H_2O$ was used to adjust the pH value of the solution to 7–8. The solution containing the complex precursor was then heated on a hot plate at ~523 K to form a black, soft and fluffy product. Finally, the product was calcined in air at 1173 K for 5 h to prepare LNO oxide.

2.2. Membrane preparation

A dry pressing technique and co-sintering route [15] were utilized to prepare the supported dense mixed-conducting membranes. An ABB′B″B′BA-type membrane, with two dense membrane layers and five porous support layers, was prepared. Appropriate amounts of membrane material (LNCO) were first poured into a stainless die. The surface of the membrane material was leveled off at an intermediate pressure of 60 MPa. After holding under the load for several minutes, the pressure was released and then five layers of support material (LNO) together with the 5–25 wt.% of the active carbon, which acted as the porous former, were added onto the surface of the membrane material layer by layer in the order of 5, 15, 25, 15 and 5 wt.%. Each layer of the support needed to be leveled off at about 60 MPa and held for several minutes. After the fifth layer of the support had been completed, appropriate amounts of membrane material were added on to the surface of the support material. A pressure of 240 MPa was applied to form the green supported membranes with a sandwich structure and a diameter of 16 mm. Finally, the green supported membranes were sintered at 1523 K for 2 h. As the temperature rose, the support shrunk at a rate close to that of the membrane layer. Meanwhile, with the increase in temperature, the active carbon burned out to form many pores in the support. The removal of the active carbon provided the higher porosity in the support than in the membrane layer. After sintering, supported membranes were obtained with a dense and defect-free membrane layer and a pore-gradient structure support layer. Before using as a membrane reactor, the supported membrane was cut into two ABB′B″-type membranes with a dicing cutter (EC400, Kejing, ShenYang, China). The complete process for preparing the ABB′B″-type membrane is shown in Fig. 2. In order to simplify the narration, the symbols LNO-5, LNO-15 and LNO-25 were used to denote the different support layers that contained 5, 15 and 25 wt.% active carbon. The thickness of every layer of the supported membrane was controlled by the amount of the added materials.

For the comparison of membrane performance, a dense symmetric LNCO membrane and an AB-type membrane were also prepared under identical conditions to that of the ABB′B″-type membrane.

2.3. Characterization

The crystal structures of the samples were characterized by X-ray diffraction (XRD, D8-advance, Bruker, Germany) using Cu Kα radiation. The experimental diffraction patterns were collected at room temperature by step scanning in the range $20^\circ \le 2\theta \le 80^\circ$ with an increment of 0.05°. The sintering behaviors of the samples were investigated by a dilatometer (NETZSCH DIL 402C) in still air to 1523 K at a heating rate of 2 K min^{-1}. The morphology of the supported mixed-conducting membrane was examined by scanning electron microscopy (SEM) (FEI, Model Quanta-2000, Holland). The working parameters of the SEM are as follows: high voltage (HV) 25–30 kV, work distance (WD) 8–10 mm and Spot 3.0. The surface chemical composition of the support before and after POM was analyzed by X-ray photoelectron spectroscopy (XPS) (PerkinElmer, PHI-550 ESCA/SAM, USA), equipped with an Al Kα X-ray source ($h\nu$ = 1486.6 eV). The pressure in the ion-pumped analysis chamber was below 1.0×10^{-6} Pa. All binding energies (BE) were referenced to the adventitious C 1s line at 284.6 eV. This reference gave BE values with an accuracy of ±0.1 eV.

2.4. Membrane reactor set-up

The membrane reactor module and experimental apparatus for hydrogen production was described in our previous work [16]. The

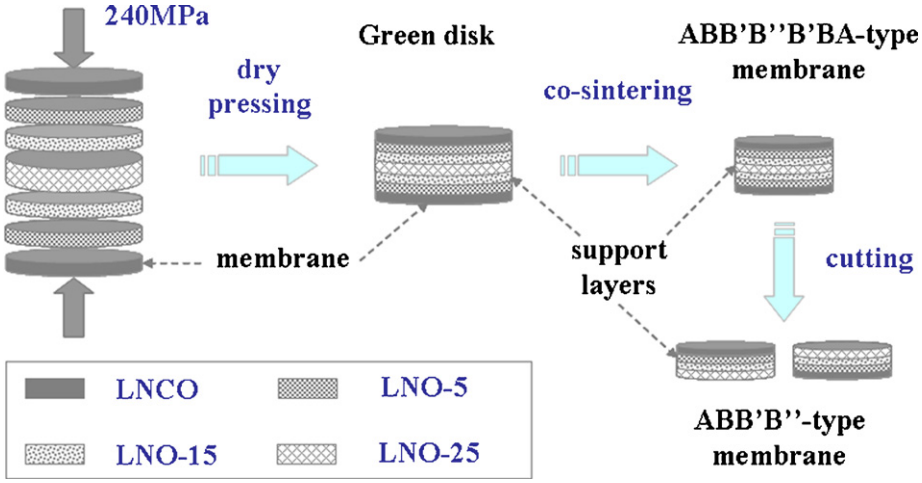

Fig. 2. Preparation procedure for the supported mixed-conducting membrane.

membrane disk was sealed between two gold rings and the edge of the disk was surrounded with ceramic sealant. The effective area of the membrane for oxygen permeation was about 0.283 cm^2. Before starting the POM reaction, the assembly was heated from room temperature to 1313 K at 2 K min^{-1} and held for 4 h to ensure the softening of the gold rings. Gas leakage, if present, could be detected by monitoring the nitrogen concentration in the effluent from the support side. The inlet gas flow rates were controlled by mass flow controllers (Models D07/ZM, Beijing Jianzhong Machine Factory, China), which were calibrated by a bubble flowmeter. Both sides of the membrane were maintained at atmospheric pressure. A programmable temperature controller (Model AI-708PA, Xiameng Yudian automation technology Co., Ltd.) was utilized to monitor the temperature around the membrane.

Air was introduced to the membrane layer surface and CH_4, together with He, was introduced to the porous support surface. The flow rates of air, CH_4 and He were 100, 2.0 and 18.0 ml(STP) min^{-1}, respectively. The effluent streams were analyzed by two on-line gas chromatographs (Shimadzu Model GC-8A, Japan). A 5 A molecular sieve column of 2 m was used for the separation of H_2, O_2, N_2, CH_4 and CO, and a TDX-01 column of 1 m was used for separating CO_2 and hydrocarbons. The chromatograph with 5 A molecular sieve was operated under a current of 180 mA and the attenuation of 1, conditions under which a trace amount of oxygen (>1 Pa) could be detected. The analyses were checked by the carbon balance, which was within 5% for all reaction experiments. For oxygen permeation measurements, helium gas (30 ml(STP) min^{-1}) was used as the sweeping gas in the permeation side, and an internal standard gas CH_4 (about 1.0 ml(STP) min^{-1}) was added to the effluent streams and passed through the on-line analysis loop. In the membrane reaction experiments, methane diluted by helium was introduced into the reaction side of the membrane, and the unreacted feed gases and products passed through the loop of the on-line analysis.

The conversion of CH_4, selectivity and production of H_2 for the POM were defined, respectively, as follows:

$$X_{CH_4} = \frac{F_{CH_4 inlet} - F_{CH_4 outlet}}{F_{CH_4 inlet}} \quad (4)$$

$$S_{H_2} = \frac{F_{H_2}}{2(F_{CH_4 inlet} - F_{CH_4 outlet})} \quad (5)$$

$$P_{H_2} = \frac{2X_{CH_4} S_{H_2} F_{CH_4 inlet}}{A_m} \quad (6)$$

where X_{CH_4} is the conversion of CH_4, S_{H_2} and P_{H_2} are selectivity and production of H_2 for the POM, respectively. F_i is the flow rate of species i, in mol s^{-1}. The oxygen flux in the membrane reactor could be calculated by the mass balance on the basis of the components of CO, CO_2, O_2 and H_2O in the exit stream:

$$F_{O_2 inlet} = F_{O_2 outlet} + \frac{1}{2}F_{CO} + F_{CO_2} + \frac{1}{2}F_{H_2O} \quad (7)$$

where F_{H_2O} can be calculated based on the hydrogen balance as follows:

$$F_{CH_4 inlet} = F_{CH_4 outlet} + \frac{1}{2}F_{H_2} + \frac{1}{2}F_{H_2O} \quad (8)$$

Substitution of Eq. (8) into Eq. (7) yields:

$$F_{O_2 inlet} = F_{O_2 outlet} + \frac{1}{2}F_{CO} + F_{CO_2} + F_{CH_4 inlet} - F_{CH_4 outlet} - \frac{1}{2}F_{H_2} \quad (9)$$

3. Results and discussion

3.1. Sintering behaviors of membrane and porous support

For the co-sintering method, it is crucial for the support layers to have similar sintering behavior to the membrane layers in order to obtain a dense, crack-free supported membrane. In other words, during the densification process of the supported membrane, the dimensions of the support layers should undergo a similar change to those of the membrane layers. The sintering behaviors of membrane and support layers (with various amounts of active carbon) were investigated individually by a dilatometer and the results are presented in Fig. 3. It can be seen that the sintering behavior of LNCO is quite different to that of LNO-5, LNO-15 and LNO-25 in the temperature range 750–1523 K. LNCO begins to shrink at about 1323 K and the linear shrinkage is 14% at 1523 K. In contrast, the onset shrinkage temperatures of the LNO-5, LNO-15 and LNO-25 are about 1173 K and the linear shrinkage are 14.5, 19.3 and 23.5%, respectively, at 1523 K. The ABB′B″-type membrane (with a membrane layer and three support layers), is therefore difficult to prepare successfully with a direct dry pressing and co-sintering technology. The experimental results show that the ABB′B″-type membrane is prone to bend during sintering. This result can be explained by the stress state analysis of the membrane layer and support layers during sintering. From Fig. 3, the support layers begin to shrink at about 1173 K, whereas the membrane layer does not shrink at this temperature. The large sintering stress in the support layers causes a compressive stress at the bottom of the membrane

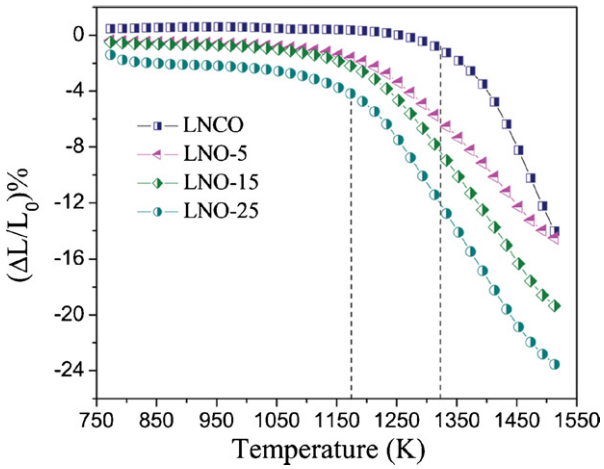

Fig. 3. Sintering behavior of the LNCO membrane and LNO support layers (with various amounts of active carbon).

layer. This compressive stress leads to the bending of the whole supported membrane (see Fig. 4). The bending of the membrane layer results in a large space between powders in the membrane, which is disadvantageous for the densification of the membrane. As seen in the inset of Fig. 4, the surface of the curved membrane is porous.

3.2. Formation of the supported dense mixed-conducting membrane

In order to avoid this mismatch of sintering behavior between the membrane and support, an ABB′B″B′BA-type membrane, with two dense membrane layers and five porous support layers, was prepared. The symmetric stress in this type of membrane during the sintering process ensures successful preparation of a dense and crack-free supported membrane.

Fig. 5 shows the SEM micrograph of the ABB′B″-type membrane (cutting from ABB′B″B′BA-type membrane), which consists of a LNCO membrane layer and LNO-5, LNO-15 and LNO-25 as support layers. ML, SL1, SL2 and SL3 refer to the membrane layer, LNO-5 support layer, LNO-15 support layer and LNO-25 support layer, respectively. It can be seen that the membrane with a thickness of about 120 μm is well bonded to the support, and the support is porous (Fig. 5a). The surface of the membrane is dense and crack-free and ceramic grains with clear grain boundaries are visible (Fig. 5b). The porosity of the support increases with increasing amounts of active carbon (Fig. 5SL1–SL3). As for the supported membrane, the porous support layers should have high porosity and low gas transport resistance so that the net transport rate is not determined by the diffusion of gas in the support. However, the mechanical strength of the membrane deceases with increasing porosity of the support. Therefore, a pore-gradient structure support was designed in this work to achieve not only low gas transport resistance, but also high mechanical strength.

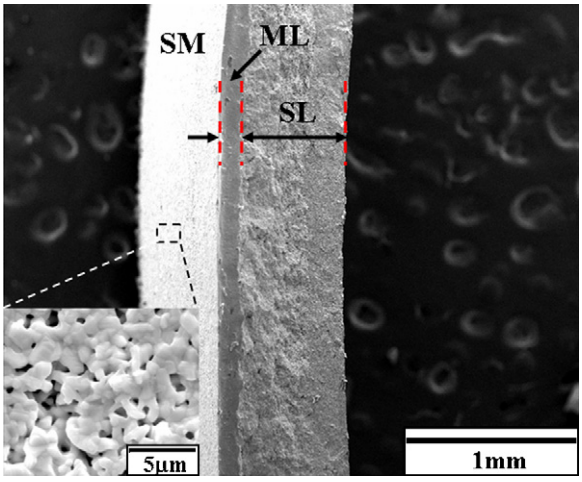

Fig. 4. SEM images of the curved ABB′B″-type membrane prepared by a direct dry pressing and co-sintering route. The inset shows the surface microstructure of the curved membrane. SM, ML and SL refer to the surface of the membrane, the membrane layer and the porous support layer, respectively.

3.3. Oxygen permeability of the supported dense mixed-conducting membrane

In the POM reaction, the consumption of 1 mol O_2 will produce 4 mol H_2, so the oxygen permeability of the membrane is a significant factor in the production rate of hydrogen. The ABB′B″-type membrane with a membrane layer 120 μm thick and the whole porous layer about 880 μm thick (LNO-5 ≈ 250 μm; LNO-15 ≈ 250 μm; LNO-25 ≈ 380 μm) was applied to evaluate the oxygen permeability. For comparison, the oxygen fluxes of an AB-type membrane, which had a 120 μm LNCO membrane layer and an 880 μm LNO-15 porous support layer, and a symmetric 1 mm LNCO membrane were also tested under identical experimental conditions. Measurements were made between 1073 and 1223 K at an oxygen partial pressure gradient of $2.1 \times 10^4/1 \times 10^2$ Pa. As shown in Fig. 6, the oxygen flux of the ABB′B″-type membrane is greater than that of the AB-type membrane and symmetric LNCO membrane. At 1173 K, the oxygen flux of the ABB′B″-type membrane is 5.44×10^{-7} mol cm^{-2} s^{-1}, which is about 5.6 times that of the symmetric LNCO membrane and 1.6 times that of the AB-type membrane.

For a dense mixed-conducting membrane, the oxygen permeation rate is controlled by two factors: the rate of oxygen ion diffusion within the bulk and the oxygen surface exchange on each side of the membrane [17]. Therefore, the preparation of the supported membrane is an effective way to reduce the membrane thickness and improve the oxygen flux. In addition, for a thin dense ceramic membrane (e.g. a supported membrane), the surface exchange rate is often the main factor determining the oxygen flux. Further increase in the permeability of this membrane can result from the surface activation, which would promote a faster surface oxygen exchange reaction because of the enhanced catalytic activity and increased effective area. This viewpoint is commonly accepted and the surface activation methods are widely used to enhance the surface oxygen change rate [18–20]. In this work, the oxygen flux through an ABB′B″-type membrane is dramatically improved by a decrease of the membrane thickness. Furthermore, the porous LNO catalyst layer coating on the dense LNCO thin membrane increases the effective area for the surface oxygen exchange reaction (the oxidation of oxygen ions to oxygen molecules). Considering the high surface exchange coefficients of LNO oxide [21], we can state that the oxygen flux of the ABB′B″-type membrane is also improved by the porous LNO support layers. However, the contribution of the porous LNO layers to the overall oxygen permeability also depends on the thickness and microstructure of the porous layers, which determines whether they have a positive effect on the overall oxygen permeability. This is the reason why the oxygen flux of an ABB′B″-type membrane is higher than that of an AB-type membrane. The preparation of a pore-gradient support layer is the beginning of a program of work to optimize the porous support layer. Further work is important and necessary.

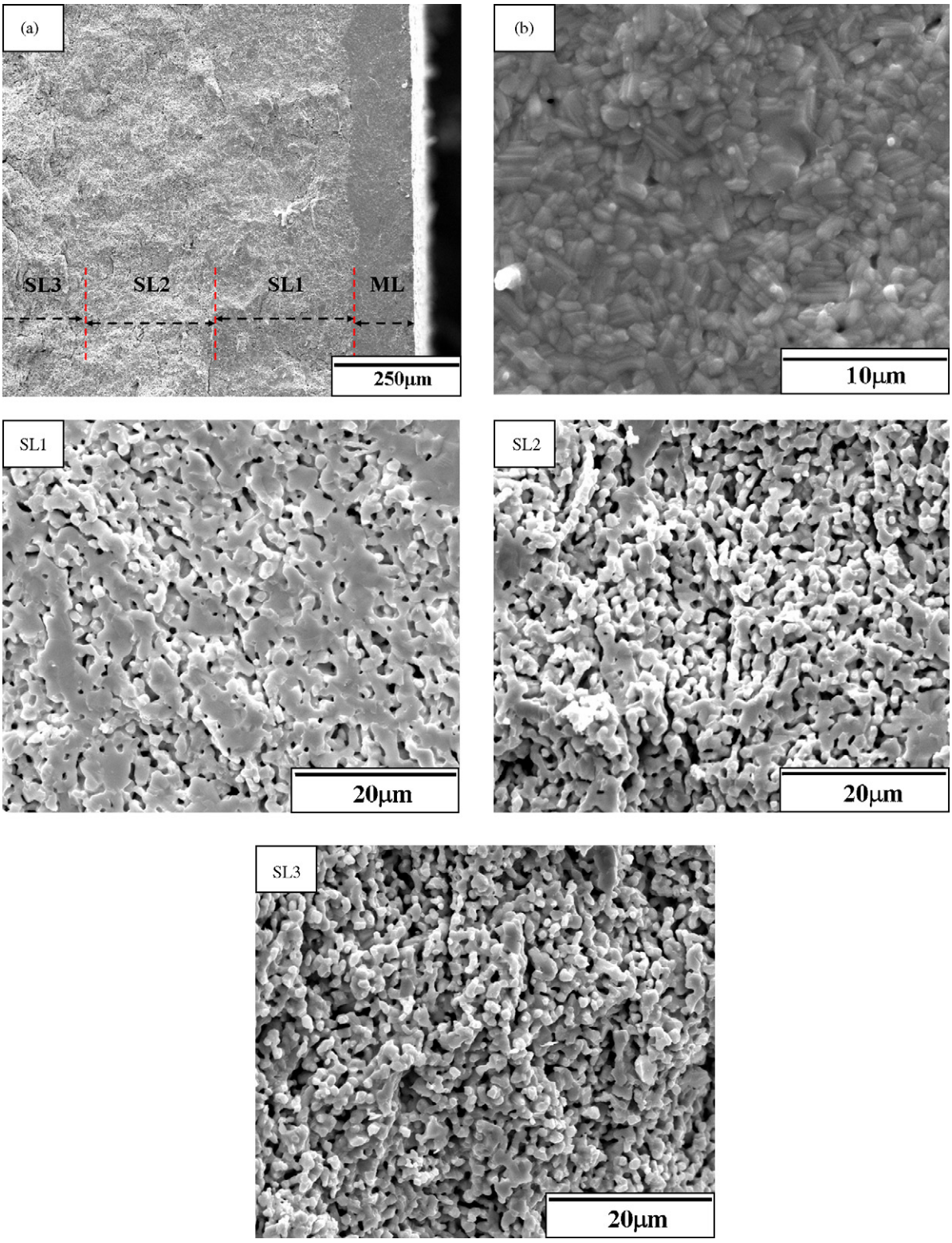

Fig. 5. SEM micrographs of the cross-section (a) and surface (b) of the dense and crack-free ABB′B″-type membrane. ML, SL1, SL2 and SL3 refer to the membrane layer, LNO-5 support layer, LNO-15 support layer and LNO-25 support layer, respectively.

3.4. A self-catalytic membrane reactor for effective hydrogen production

Because of the high catalytic activity and stability of the LNO oxide for the methane reforming reaction [12,22], hydrogen can be produced via a self-catalytic membrane reactor constructed as an ABB′B″-type membrane. At the beginning of the reaction, the effect of methane concentration on the membrane reactor performance was investigated. Because helium was used as a sweep gas, we did not use pure methane as the feed gas. In this experiment, the flow

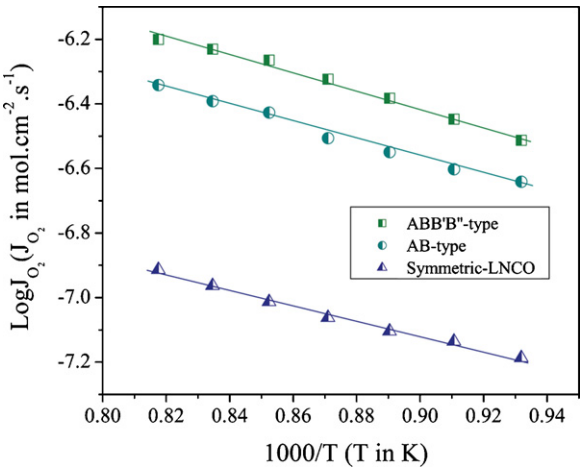

Fig. 6. Temperature dependence of the oxygen permeation fluxes of the ABB′B″-type membrane, AB-type membrane, and symmetric LNCO membrane. The upstream and downstream oxygen partial pressures are 2.1×10^4 and 1×10^2 Pa, respectively. The thickness of each membrane is 1.0 mm.

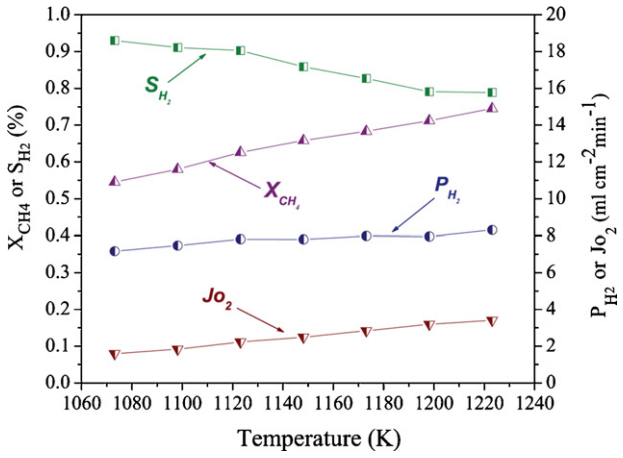

Fig. 8. H_2 selectivity, H_2 production, CH_4 conversion, and O_2 permeation flux as a function of temperature in the self-catalytic membrane reactor. Reaction side: He = 18 ml(STP) min^{-1}, CH_4 = 2.0 ml(STP) min^{-1}; air side: air = 100 ml(STP) min^{-1}; effective membrane area = 0.283 cm^2.

rate of helium was fixed at about 18 ml min^{-1} while the methane flow rate was increased from 1.5 to 3.0 ml min^{-1}. The reaction performance versus methane concentration at 1123 K is presented in Fig. 7. It shows that with increasing methane concentration, the hydrogen selectivity (S_{H_2}) remains almost constant (at around 89%) and both the hydrogen production (P_{H_2}) and oxygen flux (J_{O_2}) increases. However, the conversion of CH_4 (X_{CH_4}) decreases rapidly with increasing methane concentration. These results can be explained as follows. The oxygen partial pressure in the reaction side slightly decreased with increasing methane concentration. So, the oxygen permeation flux slightly increased. Correspondingly, the reacted methane will slightly increase with increasing oxygen permeation flux. As presented in Eq. (4), the methane conversion (X_{CH_4}) can be expressed as the ratio of the reacted methane to the feed methane. Although the reacted methane slightly increases, the feed methane increases rapidly with increasing methane concentration. So, the methane conversion decreased drastically with increasing methane concentration. Similar results were reported by Tsai et al. [23], Jin et al. [10] and Ikeguchi et al. [24]. As a result, we used 10 vol.% CH_4 (i.e. CH_4/He = 2.0/18.0 ml min^{-1}) as the feed gas for these measurements. As well as the methane concentration, the temperature is another crucial factor that will affect the membrane performance. Fig. 8 shows the temperature dependence of membrane reactor performance. Each temperature was held constant for about 2 h and the corresponding data points were recorded at least three times to ensure the accuracy of the results. The oxygen flux and CH_4 conversion increase with increasing temperature. At 1173 K, the oxygen flux is about 2.84 ml(STP) cm^{-2} min^{-1}, which is 3.9 times that measured in the air/He atmosphere; the CH_4 conversion is about 68.3%. The hydrogen production increases slightly while the hydrogen selectivity decreases with increasing temperature. At 1173 K, the hydrogen production is about 8.0 ml(STP) cm^{-2} min^{-1}. The hydrogen selectivity is better at lower temperature, and greater than 90% below 1123 K. The decrease of the H_2 selectivity can be explained as follows. The oxygen permeation flux increased with increasing the temperature. However, the flow rate and concentration of the feed methane was not adjusted. So, the CH_4/O_2 decreased at high temperatures, which led to the further oxidation of H_2 and CO to be H_2O and CO_2. Indeed, a small amount of CO_2 and H_2O can be detected in the effluent from the reforming side. Ji et al. [25] also reported that H_2 selectivity decreased with decreasing the CH_4/O_2. Therefore, the H_2 selectivity decreased with increasing the temperature. From the literatures, similar results and explanations were reported by many researchers [24,26–28].

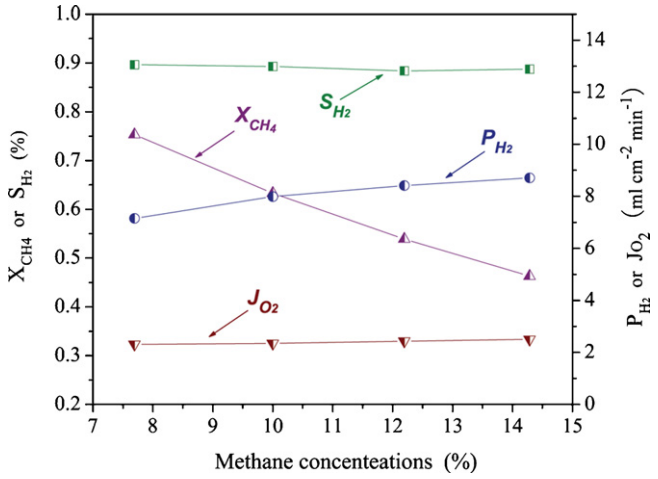

Fig. 7. H_2 selectivity, H_2 production, CH_4 conversion, and O_2 permeation flux as a function of methane concentration in the self-catalytic membrane reactor at 1123 K. Reaction side: He = 18 ml(STP) min^{-1}, CH_4 = 1.5–3.0 ml(STP) min^{-1}; air side: air = 100 ml(STP) min^{-1}; effective membrane area = 0.283 cm^2.

3.5. Long-term stability of the self-catalytic membrane reactor

For practical applications, the membrane reactor must exhibit long-term stability at elevated temperatures in reducing atmospheres. Fig. 9 shows the stability of the self-catalytic membrane reactor at 1123 K over more than 120 h. During this period the CH_4 conversion, hydrogen selectivity and hydrogen production remained at about 60%, 89% and 8.0 ml(STP) cm^{-2} min^{-1}, respectively. The oxygen flux increased slightly from 2.3 to 2.6 ml(STP) cm^{-2} min^{-1}. These results suggest that the self-catalytic process for hydrogen production is feasible and the self-catalytic membrane reactor exhibits high performance and good stability for hydrogen production. When the reaction at 1123 K had continued for about 125 h, the experiment was voluntarily stopped. The temperature of the reactor was then allowed to cool to room temperature. No cracks were found in the supported membrane. To provide further evidence of the self-catalytic reaction

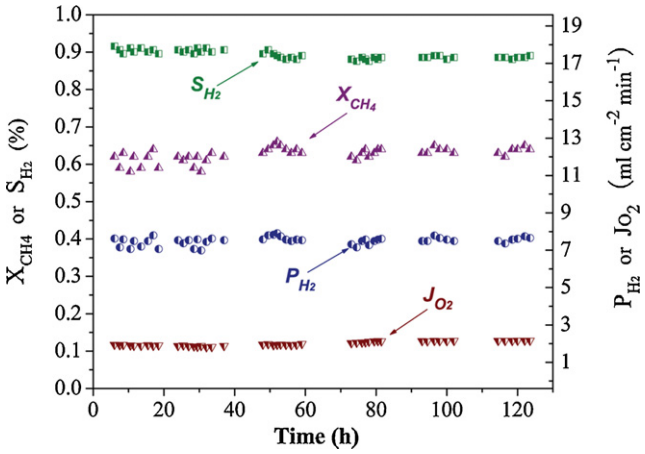

Fig. 9. H_2 selectivity, H_2 production, CH_4 conversion, and O_2 permeation flux as a function of time in the self-catalytic membrane reactor at 1123 K. Reaction side: He = 18 ml(STP) min^{-1}, CH_4 = 2.0 ml(STP) min^{-1}; air side: air = 100 ml(STP) min^{-1}; effective membrane area = 0.283 cm^2.

process that took place on the support side, the chemical state of the elements on the surface of support layer before (sample a) and after (sample b) reaction were analyzed by X-ray photoelectron spectra (XPS). As shown in Fig. 10, the Ni^0 signal (at 852.3 eV [29]) was enhanced after the reaction, which indicated that some of the nickel on the support surface had been reduced to the metallic form. This conclusion was also supported by XRD analysis. As shown in Fig. 11, Ni^0 diffraction peaks can be observed clearly in the XRD patterns of the support surface after reaction. These results confirmed that the self-catalytic reaction indeed took place.

The high performance of the self-catalytic membrane reactor may be attributed to two aspects. Firstly, as discussed in Section 3.3, the oxygen permeability of the membrane reactor is improved by the application of the ABB′B″-type membrane. Secondly, the catalytic activity of the membrane reactor is enhanced by the porous LNO layers. Compared with conventionally supported Ni catalysts, the reduced Ni^0 from LNO are dispersed at the atomic-scale on the surface of the support layer. Furthermore, during the POM reaction, the LNO was partially reduced by the reducing atmosphere ($CO + H_2$) to NiO and even to Ni^0, and Ni^0 was partially oxidized by the oxygen permeating from the air side. A redox

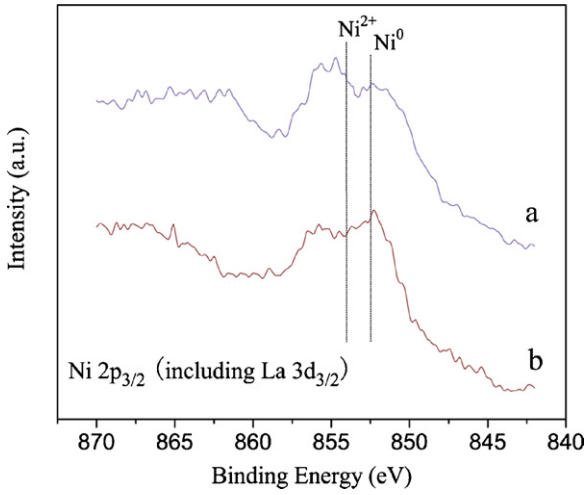

Fig. 10. Nickel $2p_{3/2}$ XPS spectra (including La $3d_{3/2}$ contribution) of the porous support layer (LNO): (a) before and (b) after reaction for more than 120 h.

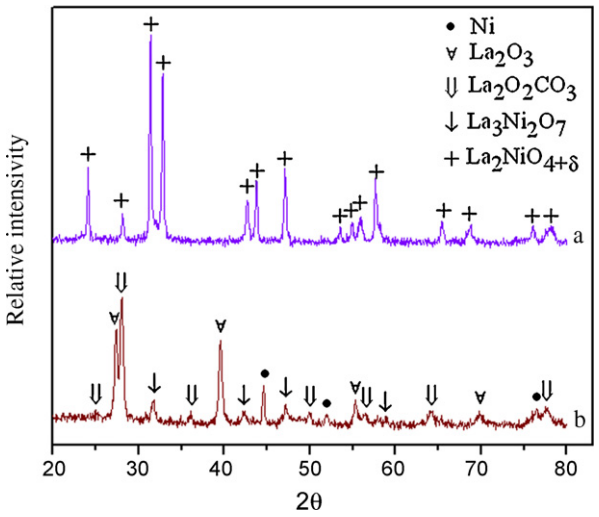

Fig. 11. The XRD patterns of the porous support layer (LNO): (a) before and (b) after reaction for more than 120 h.

equilibrium was finally attained between the catalyst and the reactant stream [30]. This reversibility of the Ni catalyst avoided the agglomeration and grain growth of Ni^0 during the reaction process, which improved the catalytic stability of the membrane reactor. Liu and Au [12], Guo et al. [22] and Zheng and coworkers [31] also reported that LNO possessed higher catalytic activity and stability than the supported Ni catalysts in the methane reforming reactions.

4. Conclusions

A crack-free supported mixed-conducting LNCO membrane was successfully prepared via dry pressing technology on a LNO support with pore-gradient structure, followed by sintering. The match of sintering behaviors between the membrane and support was realized by the preparation of an ABB′B″B′BA-type membrane. An SEM test demonstrated that the surface of the supported membrane was dense and crack-free, the thickness of the membrane was about 120 μm and the pore-gradient structure of the support can be observed clearly. At 1173 K, the oxygen flux of the ABB′B″-type membrane is 5.44×10^{-7} mol cm^{-2} s^{-1}, which is about 5.6 times that of the symmetric LNCO membrane and 1.6 times that of the AB-type membrane. A self-catalytic mixed-conducting membrane reactor derived from the prepared supported membrane was constructed for hydrogen production from methane. It was found that this membrane reactor exhibited high performance and good stability for hydrogen production. At 1123 K, the CH_4 conversion, hydrogen selectivity and hydrogen production remained at about 60%, 89% and 8.0 ml(STP) cm^{-2} min^{-1}, respectively, for more than 120 h. The concept for the novel self-catalytic membrane reactor can also be utilized for the design and preparation of a high efficiency catalytic membrane reactor.

Acknowledgements

This work was supported by the National Basic Research Program of China (No. 2003CB615702), National Natural Science Foundation of China (Nos. 20636020, 20436030), Innovation Foundation for Doctoral Dissertation (No. BSCX200709). The National High Technology Research and Development Program (2006AA030204), and the Natural Science Foundation of Jiangsu Province (BK2006722) of China.

References

[1] R. O'Hayre, S.W. Cha, W. Colella, F.B. Prinz, Fuel Cell Fundamentals, John Wiley & Sons, New York, 2006, pp. 292–306.
[2] S. Rakass, H. Oudghiri-Hassani, P. Rowntree, N. Abatzoglou, J. Power Sources 158 (2006) 485–496.
[3] Z.W. Liu, K.W. Jun, H.S. Roh, S.E. Park, J. Power Sources 111 (2002) 283–287.
[4] Y.S. Seo, D.J. Seo, Y.T. Seo, W.L. Yoon, J. Power Sources 161 (2006) 1208–1216.
[5] D. Kennedy, Science 305 (2004) 917.
[6] L.W. Chen, Q. Hong, J.Y. Lin, F.M. Dautzenberg, J. Power Sources 164 (2007) 803–808.
[7] J.G. Seo, M.H. Youn, K.M. Cho, S. Park, I.K. Song, J. Power Sources 173 (2007) 943–949.
[8] Y. Echegoyen, I. Suelves, M.J. Lazaro, R. Moliner, J.M. Palacios, J. Power Sources 169 (2007) 150–157.
[9] D.A. Hickman, L.D. Schmidt, Science 259 (1993) 343–346.
[10] W.Q. Jin, S.G. Li, P. Huang, N.P. Xu, J. Shi, Y.S. Lin, J. Membr. Sci. 166 (2000) 13–22.
[11] X.L. Dong, C. Zhang, X.F. Chang, W.Q. Jin, N.P. Xu, AIChE J. 54 (2008) 1678–1680.
[12] B.S. Liu, C.T. Au, Catal. Lett. 85 (2003) 165–170.
[13] C. Batiot-Dupeyrat, G. Valderrama, A. Meneses, F. Martinez, J. Barrault, J.M. Tatibouët, Appl. Catal. A: Gen. 248 (2003) 143–151.
[14] X.L. Dong, Z. Xu, X.F. Chang, C. Zhang, W.Q. Jin, J. Am. Ceram. Soc. 90 (2007) 3923–3929.
[15] X.F. Chang, C. Zhang, W.Q. Jin, N.P. Xu, J. Membr. Sci. 285 (2006) 232–238.
[16] X.H. Gu, W.Q. Jin, C.L. Chen, N.P. Xu, J. Shi, Y.H. Ma, AIChE J. 48 (2002) 2051–2060.
[17] H.J.M. Bouwmeester, A.J. Burggraaf, in: A.J. Burggraaf, L. Cot (Eds.), Fundamentals of Inorganic Membrane Science and Technology, Elsevier Science B.V., Amsterdam, 1996, pp. 435–528.
[18] T.H. Lee, Y.L. Yang, A.J. Jacobson, B. Abeles, S. Milner, Solid State Ionics 100 (1997) 87–94.
[19] V.V. Kharton, A.V. Kovalevsky, A.A. Yaremchenko, F.M. Figueiredo, E.N. Naumovich, A.L. Shaulo, F.M.B. Marques, J. Membr. Sci. 195 (2002) 277–287.
[20] S. Lee, K.S. Lee, S.K. Woo, J.W. Kim, T. Ishihara, D.K. Kim, Solid State Ionics 158 (2003) 287–296.
[21] S.J. Skinner, J.A. Kilner, Solid State Ionics 135 (2000) 709–712.
[22] C.L. Guo, X.L. Zhang, J.L. Zhang, Y.P. Wang, J. Mol. Catal. A: Chem. 269 (2007) 254–259.
[23] C.Y. Tsai, A.G. Dixon, W.R. Moser, Y.H. Ma, AIChE J. 43 (1997) 2741–2750.
[24] M. Ikeguchi, T. Mimura, Y. Sekine, E. Kikuchi, M. Matsukata, Appl. Catal. A: Gen. 290 (2005) 212–220.
[25] Y.Y. Ji, W.Z. Li, H.Y. Xu, Y.X. Chen, Appl. Catal. A: Gen. 213 (2001) 25–31.
[26] D. Bayraktar, F. Clemens, S. Diethelm, T. Graule, J. Van herle, P. Holtappels, J. Eur. Ceram. Soc. 27 (2007) 2455–2461.
[27] H.H. Wang, C. Tablet, A. Feldhoff, J. Caro, Adv. Mater. 17 (2005) 1785–1788.
[28] Z.P. Shao, G.X. Xiong, H. Dong, W.S. Yang, L.W. Lin, Sep. Purif. Technol. 25 (2001) 97–116.
[29] J.F. Moulder, W.F. Stickle, P.E. Sobol, K.D. Bomben, Handbook of X-ray Photoelectron Spectroscopy, PerkinElmer, Minnesota, 1992, pp. 84–85.
[30] Y.H. Hu, E. Ruckenstein, Adv. Catal. 48 (2004) 297–345.
[31] J.J. Guo, H. Lou, Y.H. Zhu, X.M. Zheng, Mater. Lett. 57 (2003) 4450–4455.